Nonisolated Single-Switch Two-Channel LED Driver with Simple Lossless Snubber and Low-Voltage Stress

Jong-Woo Kim, *Member, IEEE*, Jung-Muk Choe, *Member, IEEE*, and Jih-Sheng (Jason) Lai, *Fellow, IEEE*

***Abstract*—In two-channel light-emitting diode (LED) driver, capacitive-current-balancing method is the simplest and the most effective way to equally balance the current in each channel due to its simplicity. As a result, the capacitive balancing method was used with flyback or tapped-boost converters in low-power LED applications. Since flyback and tapped-boost converters suffer from a snubber loss and a high-voltage stress on the switching devices, conventional approaches use additional passive components, resulting in the limitations on the cost and power density. In this paper, a new converter topology for low-power two-channel LED application has been proposed. The proposed converter uses the blocking capacitor and the output capacitor as a snubber capacitor so that it has a low-voltage stress without using the additional components. Although the blocking capacitor plays a role as a snubber capacitor, the current balancing characteristic is still preserved. Furthermore, the proposed converter has a high efficiency since it minimizes the number of semiconductor components in the current paths. The effectiveness of the proposed converter has been verified with an offline 3.3 V_{dc} input and 11.55 W rated output prototype.**

***Index Terms*—Capacitive current balancing, light-emitting diode (LED), regenerative snubber, two-channel LED driver.**

I. Introduction

NOWADAYS, the light-emitting diode (LED) is the most promising light source due to its long lifetime, high efficiency, and eco-friendly characteristics [1], [2]. When a number of diodes are used, they are connected in series to obtain the same luminance in each LED because the luminance of LED is related to the current. In this case, adapting two-channel structure with multi-output can achieve lower voltage stress on the switching devices compared to a single channel structure. For these reasons, many researchers have been studying the two-channel structure of LED drivers. Since each LED has its own voltage-current characteristics with negative temperature coefficient, researches on how to regulate the current on LED are essential.

Methodologies on current balancing of two-channel LED [3]–[16] driver can be divided into passive and active methods.

Manuscript received April 2, 2017; revised May 31, 2017; accepted June 27, 2017. Date of publication July 11, 2017; date of current version February 1, 2018. Recommended for publication by Associate Editor J Marcos Alonso (GE). *(Corresponding author: Jong-Woo Kim.)*

The authors are with the Future Energy Electronics Center, The Bradley Department of Electrical and Computer Engineering, Virginia Tech, Blacksburg, VA 24061 USA (e-mail: jwkim@vt.edu; jmchoe@vt.edu; laijs@vt.edu).

Color versions of one or more of the figures in this paper are available online at http://ieeexplore.ieee.org.

Digital Object Identifier 10.1109/TPEL.2017.2722985

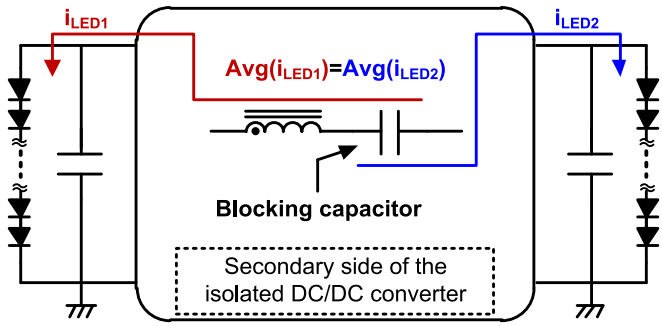

Fig. 1. Concept of the capacitive balancing method in two-channel LED driver.

Usually, passive methods can be more attractive since they do not require any semiconductor devices achieving a low cost of the system. The passive methods are subdivided into inductive and capacitive methods. The inductive methods use current-sharing transformers (CSTs) so that their current can be equally distributed. However, a careful design of the CST is required, and high-voltage stress is imposed on the devices during the reset period of CST. The capacitive methods use the charge balance condition of a blocking capacitor as shown in Fig. 1. It can be seen that the currents provided to each channel flow in the opposite directions through the blocking capacitor so that the current in each channel is naturally balanced by the charge balance condition. Due to its simple design and implementation compared to the inductive methods, the capacitive balancing method has extended its area to the small power two-channel LED driver applications [15], [16].

In conventional approaches, the small power LED drivers with a low input voltage have a relatively high output voltage to drive LED string. In these kinds of applications, it can be seen that the topologies for LED drivers are step-up converters. In small-power and step-up specifications, the flyback and the tapped-boost converter with the blocking capacitor can be strong candidates due to their high step-up capability and simplicity [15]–[19]. The flyback and tapped-boost converter has high step-up capability in that they can increase the voltage conversion ratio simply by adjusting the turns ratio of the magnetic devices. Also, they only use one switching device resulting in cost effectiveness. Furthermore, with the blocking capacitor, current sharing between two LED strings becomes simple. However, both of the flyback and tapped-boost converters suffer

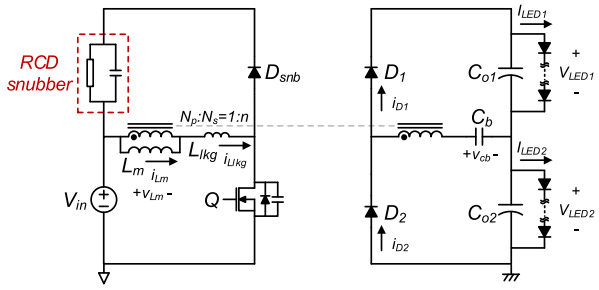

Fig. 2. Isolated forward-flyback two-channel LED driver with voltage doubler rectifier and blocking capacitor.

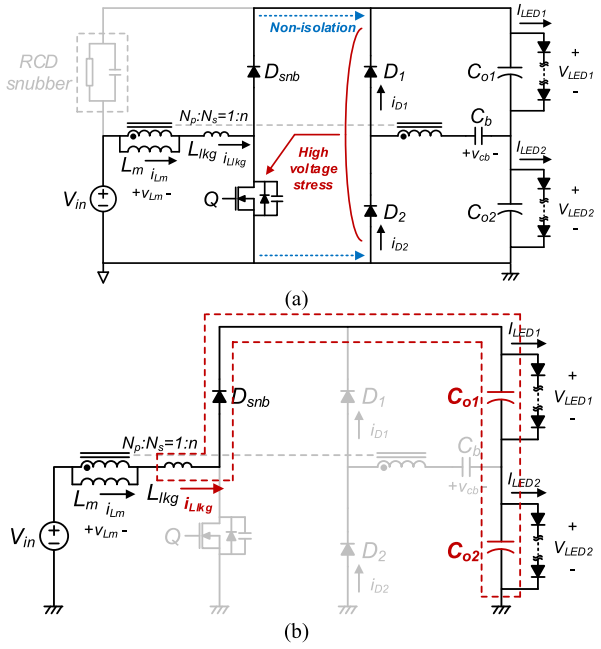

Fig. 3. (a) Derivation of nonisolated forward-flyback two-channel LED driver with RCD snubber elimination. (b) Current path of leakage inductor during the reset.

from high-voltage stress, much higher than the output voltage, on the switching devices. This is because the energy stored in the leakage inductor of the magnetic components causes a severe resonance when the switch is turned off. Regrettably, it is essential for these converters to reset the energy stored in the leakage inductor, in order to deliver the energy in the magnetizing inductor to the output. The resistor-capacitor-diode (RCD) snubber is the easiest way, but it degrades the efficiency of the converter due to the energy dissipation. To beat this problem, researchers have been studied lossless snubbers [20], [21]. These methods store the energy into the lossless snubber components and then return the energy back to the input source or deliver to the output side. Although these methods improve the efficiency, the cost and power density of the system is degraded since they require additional components.

For these reasons in this paper, it is aimed to deliver the energy stored in the leakage inductor directly to the output side, not storing in the additional components. There are some important characteristics that should be considered during the derivation of the proposed driver. First, the additional components for the losses snubber should be eliminated, in order to maximize the power density and price competitiveness. Second, since the proposed driver is used for the two-channel LED applications, the current balancing capability should be preserved. The derivation, operating principles, steady-state analysis, design guidelines, and the verification of the proposed driver will be discussed in the following sections.

II. Derivation of the Proposed Driver

The derivation of the proposed driver is based on an isolated forward-flyback converter, as shown in Fig. 2. Among many isolated converters [8]–[14], [23], [24], the forward-flyback converter is advantageous in that is uses a small number of components. A voltage doubler rectifier has been adapted in order to obtain a larger voltage conversion ratio. Also, in order to reduce the primary side current when the switch is turned off, a resonant blocking capacitor has been selected. As mentioned before, the conventional forward-flyback converter has a RCD snubber in order to reset the current in the leakage inductor.

As shown in Fig. 3(a), in nonisolated applications, the output capacitors can be used as the snubber capacitor. In the voltage doubler rectifier, two output capacitors are connected in series. Therefore, the sum of the output voltage is large enough to reset the current in the leakage inductor. During the reset, the amount of charges delivered to C_{o1} and C_{o2} are equal each other since the output capacitors for each channel are connected in series. It can be noted that the non-isolated two-channel LED driver shown in Fig. 3(a) does not require any additional component, and also the current balancing characteristic is well preserved. However, it suffers from a high-voltage stress, because the sum of the two output voltages is imposed on the main switch in this structure.

Fig. 4(a) and (b) illustrates the derivation and configuration of the proposed driver. The proposed driver also uses pre-existing capacitors so that it does not require the additional components. As can be seen in the figure, the difference is that the proposed driver uses the blocking capacitor and one output capacitor to clamp the voltage stress. The voltage stress on the switch can be decreased significantly, since the voltage on the blocking capacitor is much smaller than the output voltage. Furthermore, as shown in Fig. 4(c), the charges delivered to the blocking and one output capacitor are the same each other since they are connected in series. According to the charge balance condition of the blocking capacitor, the leakage inductor energy absorbed in the blocking capacitor should be delivered to the other output capacitor so that the current balancing characteristic is still preserved.

III. Steady-State Analysis

Figs. 5 and 6 illustrate the equivalent circuits and the steady state waveforms of the proposed driver. The proposed driver operates with a constant switching frequency. The output current is regulated using the duty cycle control. In this paper, the equivalent primary side leakage inductance L_{lkg} has been used for simplicity, and this approximation does not affect the analysis because the coupling coefficient of the transformer is high. The

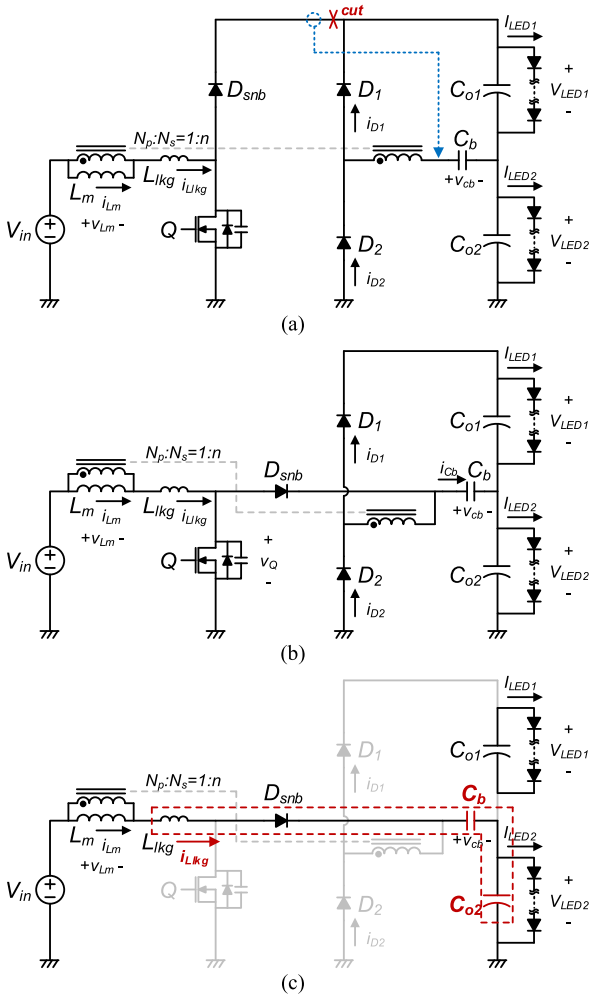

Fig. 4. (a) Derivation and (b) configuration of the proposed driver. (c) Current path of the leakage inductor during the reset.

sum of the primary side leakage inductance and the secondary side leakage inductance reflected to the primary side has been represented by L_{lkg}.

A. Operational Principle

In mode 1, during $t_0 - t_1$, Q is turned on and the resonant between L_{lkg} and C_b occurs. The current on the leakage inductor $i_{L_{lkg}}$ resonates and the voltage across C_b decreases according to the resonance. The resonant period of L_{lkg} and C_b becomes $2n\pi\sqrt{L_{lkg}C_b}$. The current on the magnetizing inductor i_{Lm} increases. Assuming the inductance of the magnetizing inductor L_m is large enough to ignore the resonance, the current on it i_{Lm} increases linearly. Since Q is turned on, the voltage across L_m and L_{lkg} is the input voltage V_{in}, and therefore, i_{Lm} increases with the slope of $V_{\text{in}}/(L_m + L_{lkg})$ and the ripple of i_{Lm} (Δi_{Lm}) becomes $V_{\text{in}}DT_s/L_m$, assuming $L_m \gg L_{lkg}$. The difference between $i_{L_{lkg}}$ and i_{Lm} is delivered to the secondary side of the transformer through D_1. Therefore, $i_{D1} = (i_{L_{lkg}} - i_{Lm})/n$ and $i_{L_{lkg}} = i_{Lm} + n_{i_{D1}}$. In the below region, $T_{\text{on}}(= DT_s)$ is large enough so that $i_{L_{lkg}}$ becomes equal to i_{Lm} and the resonance is

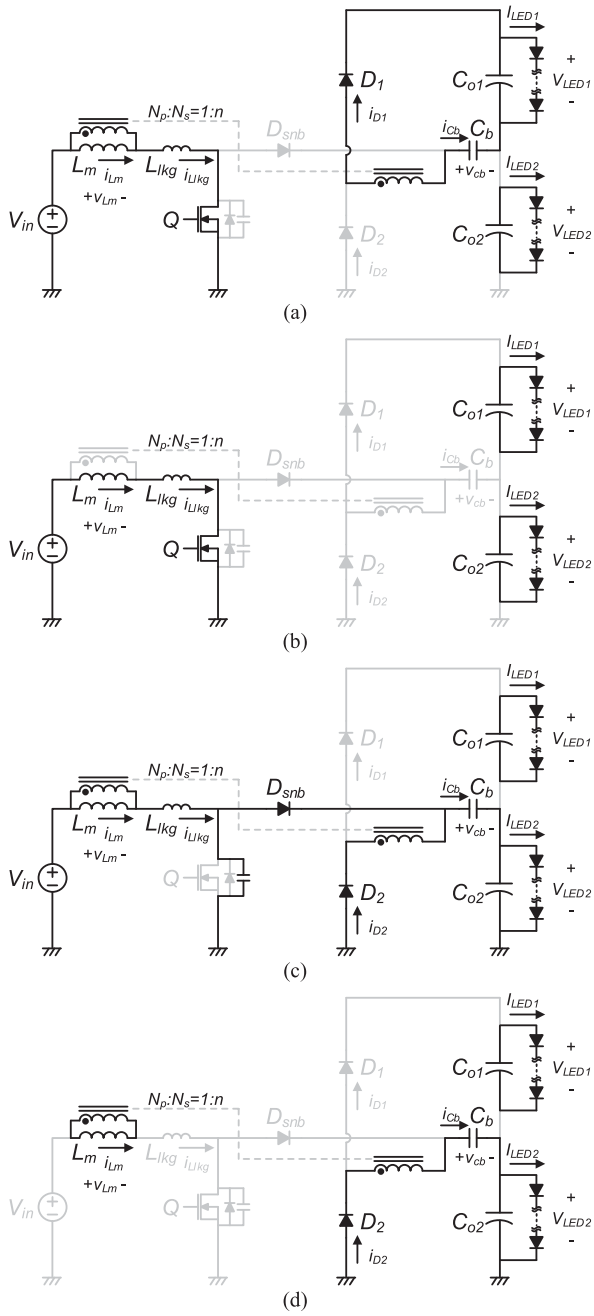

Fig. 5. Equivalent circuits of the proposed driver during: (a) mode 1 ($t_0 - t_1$), (b) mode 2 ($t_1 - t_2$), (c) mode 3 ($t_2 - t_3$), and (d) mode 4 ($t_3 - t_0'$).

finished. Mode 1 ends when either the resonant is finished in the below region or Q is turned off in the above region.

In mode 2, during $t_1 - t_2$, i_{Lm} and $i_{L_{lkg}}$ increase linearly with the slope of $V_{\text{in}}/(L_m + L_{lkg})$. This mode ends when Q is turned off.

In mode 3, during $t_2 - t_3$, after Q is turned off, the voltage across the main switch v_{ds} increases abruptly and the snubber diode D_{snb} is turned on so that v_{ds} is clamped to the sum of v_{cb} and V_{LED2}. After v_{ds} is clamped to the sum of v_{cb} and V_{LED2}, $i_{L_{lkg}}$ flows through D_{snb} thoroughly. Since C_b and C_{o2} is connected D_{snb} in series, the entire $i_{L_{lkg}}$ flows through C_b and C_{o2}. In this mode, $i_{L_{lkg}}$ is reset and the energy stored in L_{lkg} is transferred

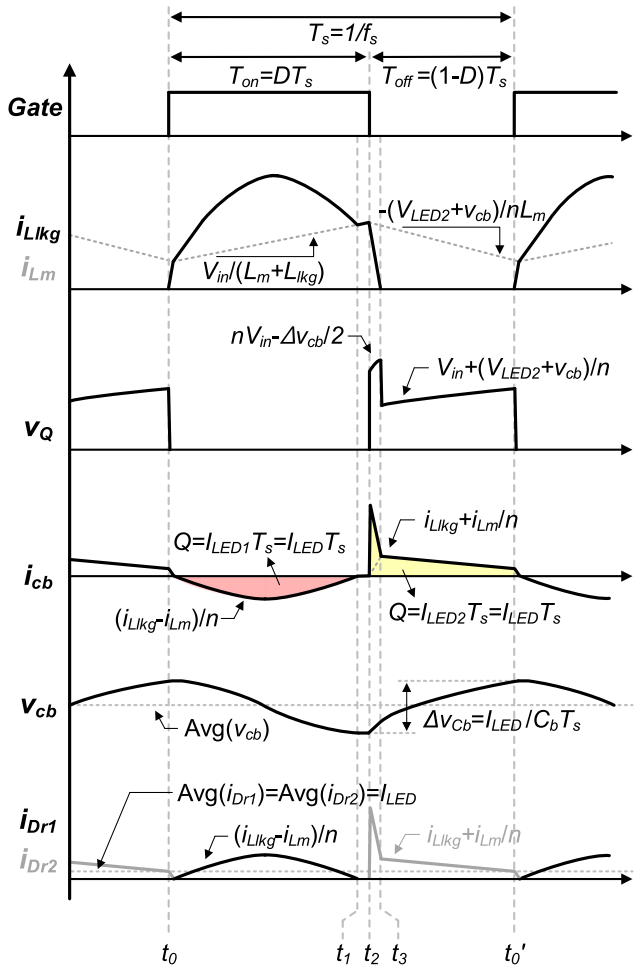

Fig. 6. The steady state waveforms of the proposed driver in a below region.

to the series connected C_b and C_{o2}, so that the amounts of the charges transferred to two capacitors are equal each other. Also, the difference between $i_{L_{lkg}}$ and i_{Lm} is transferred to the secondary side of the transformer through D_2, divided by the transformer turns ratio n. Mode 3 ends when $i_{L_{lkg}}$ becomes zero and D_{snb} is turned off.

In mode 4, during $t_3 - t_0'$, D_{snb} is turned off and the energy stored in magnetizing inductor L_m is transferred to the secondary side through D_2, divided by n. In this mode, i_{Lm} is transferred to the series connected C_b and C_{o2} so that the amounts of the energy transferred to two capacitors are also equal each other. i_{Lm} decreases by the slope of $-n(v_{cb}+V_{o2})/L_m$. Mode 4 ends when Q is turned on again. After Q is turned on, the current through D_2 decreases and the resonance between L_{lkg} and C_b begins and the proposed converter goes back to mode 1.

The proposed driver can operate in the below or above region according to the input voltage and the output current conditions. If the proposed driver operates in the below region, the resonance between the leakage inductor L_{lkg} and the resonant blocking capacitor C_b is finished before the main switch Q is turned off. On the other hand, if Q is turned off during the resonance, the proposed converter operates in the above region. In the below region, the operation of the proposed driver can be divided into four modes in a switching period T_s. In the above region, the operation of the proposed driver can be divided into three modes, excepting for mode 2 in the below region.

B. Considerations on the Current Balancing Capability

During modes 3 and 4 in the previous mode analysis, it can be noted that the output current for C_{o2} are provided by two components, $i_{L_{lkg}}$ and i_{Lm}. In the conventional flyback converter, the energy stored in L_{lkg} is not transferred to the output side because the energy is usually dissipated by RCD snubber. However, in the proposed driver, the energy stored L_{lkg} is also transferred to the output side and the current balancing capability should be studied considering $i_{L_{lkg}}$ reset. While C_{o2} is charged, C_b is always series-connected to C_{o2} so that C_b is charged by the same amount of charge with C_{o2}. According to the charge balance of the resonant blocking capacitor, the same amount of charge absorbed by C_b should be transferred in the opposite direction while C_b is discharged. Since D_1 and C_{o1} is the only current path for C_b to discharge, the same amount of absorbed by C_b is delivered to C_{o1}. Therefore, the output current for each channel is balanced equally.

C. Voltage Conversion Ratio

In order to obtain the voltage conversion ratio of the proposed driver, the average voltage on blocking capacitor $\mathrm{Avg}(v_{cb})$ should be obtained. $\mathrm{Avg}(v_{cb})$ can be obtained by the voltage-second balance condition on the secondary side of the transformer as follows:

$$\int_0^{DT_s} [V_{\mathrm{LED1}} - v_{Cb}(t)]\, dt + \int_{DT_s}^{T_s} [-V_{\mathrm{LED2}} - v_{Cb}(t)]\, dt = 0 \tag{1}$$

$$\int_0^{T_s} v_{Cb}(t)\, dt = T_{\mathrm{on}} V_{\mathrm{LED1}} - T_{\mathrm{off}} V_{\mathrm{LED2}} \tag{2}$$

$$\langle v_{Cb} \rangle = \frac{\int_0^{T_s} v_{Cb}(t)\, dt}{T_s} = DV_{\mathrm{LED1}} - (1-D)V_{\mathrm{LED2}}. \tag{3}$$

Assuming $V_{\mathrm{LED}} = V_{\mathrm{LED1}} = V_{\mathrm{LED2}}$, (2) can be rearranged as follows:

$$\langle v_{Cb} \rangle = (2D-1)\, V_{\mathrm{LED}}. \tag{4}$$

From (3), it can be noted that when $D = 0.5$ and $V_{\mathrm{LED1}} = V_{\mathrm{LED2}}$, $\langle v_{Cb} \rangle$ becomes zero. Also, $\langle v_{Cb} \rangle$ increases with a larger D and decreases with a smaller D.

It is assumed that the proposed driver operates near the resonant point, which means that Q is turned off right after the resonance between L_{lkg} and C_b ends. According to the operational principle, applying the voltage-second balance condition on L_m leads to the following equation:

$$DT_s \left[V_{\mathrm{in}} \frac{L_m}{L_m + L_{lkg}} \right] = (1-D)T_s \left[\frac{\mathrm{Avg}(v_{cb}) + V_{\mathrm{LED2}}}{n} \right]. \tag{5}$$

Rearranging (3) and (5) leads to the voltage conversion ratio of the proposed driver as follows:

$$\frac{V_{\mathrm{LED1}}+V_{\mathrm{LED2}}}{V_{\mathrm{in}}}=\frac{L_m}{L_m+L_{lkg}}\frac{n}{1-D}. \tag{6}$$

Also, assuming $L_m \gg L_{lkg}$, $L_m/(L_m+L_{lkg})$ becomes 1 and the voltage conversion ratio and the duty ratio can be approximated as follows:

$$\frac{V_{\mathrm{LED1}}+V_{\mathrm{LED2}}}{V_{\mathrm{in}}}=\frac{n}{(1-D)},\qquad D=1-\frac{nV_{\mathrm{in}}}{V_{\mathrm{LED1}}+V_{\mathrm{LED2}}}. \tag{7}$$

Assuming V_{LED} is constant, D becomes smaller as V_{in} increases.

D. Voltage Stress on the Switching Devices

Since the proposed converter has a voltage doubler rectifier, the voltage stresses on D_1 and D_2, $V_{D1\_\max}$ and $V_{D2\_\max}$, are clamped to the sum of V_{LED1} and V_{LED2} as follows:

$$V_{D1\_\max}=V_{D2\_\max}=V_{\mathrm{LED1}}+V_{\mathrm{LED2}}. \tag{8}$$

The voltage stress on the main switch is closely related to the ripple voltage of the blocking capacitor Δv_{Cb}. According to the charge balance of C_{o1}, the amount of charge delivered to C_{o1} during T_{on} is equal to $I_{\mathrm{LED1}}T_s$. Also, since C_b is connected with C_{o1} in series during T_{on}, the amount of charge delivered to C_b during T_{on} is also $I_{\mathrm{LED1}}T_s=I_{\mathrm{LED}}T_s$. In the same way, the amount of charge delivered to C_b during T_{off} is $I_{\mathrm{LED2}}T_s=I_{\mathrm{LED}}T_s$. Therefore, Δv_{Cb} can be presented as follows:

$$\Delta v_{Cb}=\frac{Q}{C_b}=\frac{I_{\mathrm{LED}}T_s}{C_b}. \tag{9}$$

From (9), it can be noted that Δv_{Cb} increases as I_{LED} increases with a given switching frequency and the blocking capacitor.

The voltage stress on the main switch $V_{Q\_\max}$ is the sum of V_{LED2} and $v_{Cb}(t_3)$. For simplicity, it is assumed that the voltage clamping period is short and C_b is large enough to neglect so that v_{Cb} is constant during t_2-t_3. In this case, v_{Cb} waveform becomes vertically symmetric and $V_{Q\_\max}$ can be presented as follows:

$$V_{Q\_\max}=V_{\mathrm{LED2}}+\langle v_{Cb}\rangle-\frac{\Delta v_{Cb}}{2}. \tag{10}$$

Substituting (3) into (10) leads to the following equation:

$$V_{Q\_\max}=D\,(V_{\mathrm{LED1}}+V_{\mathrm{LED2}})-\frac{\Delta v_{Cb}}{2}. \tag{11}$$

From (11), it can be noted that the voltage stress on the main switch is proportional to D.

E. Considerations on the Direction of N_s

An interesting feature of the proposed driver is that the voltage stress is affected by the direction of N_s. In the proposed converter, the dot side of N_s is connected to rectifier diodes. In this case, v_{Cb} decreases during DT_s since C_b is discharged.

On the other hand, when the dot side of N_s is connected to C_b, v_{Cb} increases during DT_s since C_b is charged. v_{Cb} has its maximum value when the main switch is turned off. Therefore, $V_{Q\_\max}$ becomes $D(V_{\mathrm{LED1}}+V_{\mathrm{LED2}})+\Delta v_{Cb}/2$, not $D(V_{\mathrm{LED1}}+V_{\mathrm{LED2}})-\Delta v_{Cb}/2$. In this case, the worst voltage stress occurs when I_{LED} is the maximum, and it is increased by Δv_{Cb} compared to the proposed converter. This will result in not only larger voltage stress but also larger switching loss of the main switch. This is because v_Q increases more during the turn-off transition. Therefore, in the proposed driver, it is more desirable for the dot side of N_s to be connected to rectifier diodes.

TABLE I
COMPONENTS LIST

V_{in}	2.97–3.63 V	P_{out}	11.55 W
Components	Notation	Design results	
LED	-	XREWHT-L1-0000, Cree Inc. 10EA, 5EA for each channel	
	Core	Kool Mu 77059	
Transformer	$N_p : N_s$	12(AWG16):61(AWG24), $n=5.08$	
		$J=400\ \mathrm{A/cm^2}$	
	L_m, L_{lkg}	6.25 μH, 80 nH	
Blocking cap	C_r	2.2 μF MLCC	
Output cap	C_{o1}, C_{o2}	22 μF MLCC 2EA for each	
Main switch	Q	IPB017N08N5 (70 V, 1.7 mΩ)	
Diodes	$D_{snb}D_{r1}$, D_{r2}	MBRS4201T3G (200 V)	

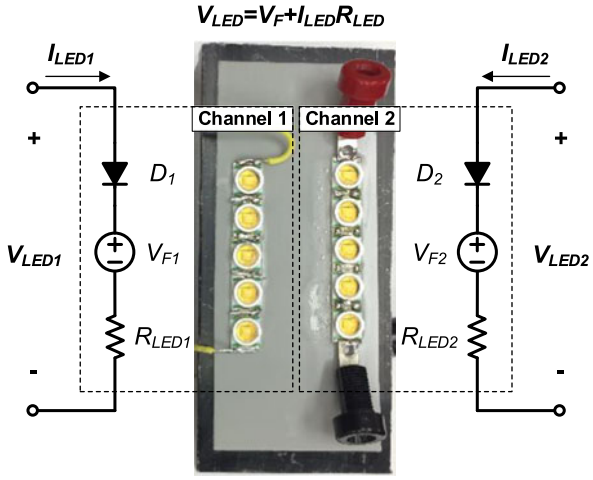

Fig. 7. Two LED channels for the experiment and their piecewise linear models.

IV. DESIGN GUIDELINES

The proposed converter has been designed for an offline $2.97-3.63\ \mathrm{V_{dc}}$ input voltage and 11.55 W (3.3 V/0.35 A LED 10EA) output two-channel LED driver. The nominal input voltage is 3.3 V and it has $\pm 10\%$ variation. Table I represents components list of the proposed driver.

A. LED Characteristics

Ten LEDs (XREWHT-L1-0000-00D01, Cree Inc.) are selected for the output. Each LED has 3.3 V/0.35 A rated output power. Fig. 7 illustrates two LED channels for the experiment and their piecewise linear models. Each channel consists of five LEDs in series, and the piecewise linear model is used with

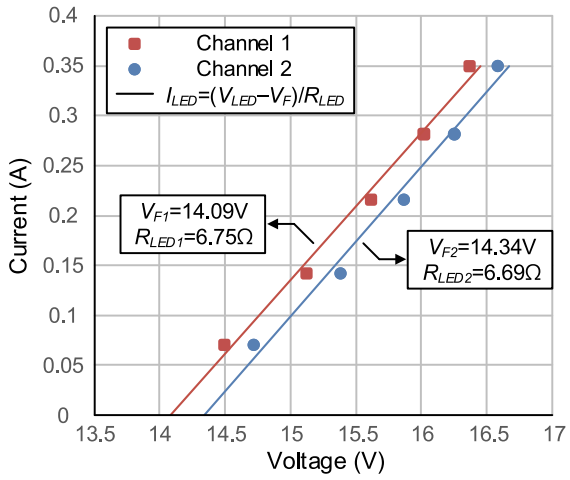

Fig. 8. *I–V* characteristics of each channels.

an ideal diode, a voltage source, and a resistor. In order to define *I–V* characteristics of LED channel, the voltages across each channel have been measured with 0.07, 0.14, 0.21, 0.28, and 0.35 A channel currents, and the data are linearly fitted. Fig. 8 illustrates the *I–V* characteristics of each channels. For channel 1, $V_{F1} = 14.09$ V and $R_{\mathrm{LED1}} = 6.75\,\Omega$, and for channel 2, $V_{F2} = 14.34$ V and $R_{\mathrm{LED1}} = 6.69\,\Omega$. In the design, the average value of two channels is used; $V_F = 14.21$ V and $R_{\mathrm{LED}} = 6.72\,\Omega$ for one channel. In this case, V_{LED} becomes 16.562 and 15.386 V at 0.35 and 0.175 A conditions, respectively.

B. Turns Ratio

Duty ratio and turns ratio determination of the proposed converter is similar with the conventional flyback converter. From (7), n increases as D increases and n decreases as D decreases in order to maintain the voltage conversion ratio with given input and output voltage. With larger n, the root-mean-square (RMS) current in the primary side can be decreased. However, increased D imposes a larger voltage stress on the main switch according to (11), resulting in larger turn-on resistance. Therefore, selection of n and D depends on the designers' choice. Usually, in the flyback converter, the maximum duty ratio can be selected near 0.5 considering efficiency optimization [22]. In this example, 0.5 duty ratio is used at the nominal input voltage and the rated output voltage condition. According to (7), n can be determined as follows:

$$n = \frac{V_{\mathrm{LED1}} + V_{\mathrm{LED2}}}{V_{\mathrm{in\_nom}}}(1-D) = \frac{2 \times 16.562}{3.3} \times 0.5 \cong 5.02. \tag{12}$$

When the output voltage becomes smaller/larger than the rated output voltage due to the tolerance, the maximum D becomes slightly smaller/larger than 0.5 at the minimum input voltage condition.

C. Transformer and Switching Frequency

In the proposed converter, the design of the magnetizing inductance of the transformer and the switching frequency is similar with the conventional flyback converter. However, since $i_{L_{lkg}}$ during T_{on} is different due to the resonant current, further discussion is required. Assuming that the efficiency of the proposed converter is 1, the input and the output power are equal as follows:

$$V_{\mathrm{in}} \frac{\int_0^{T_{\mathrm{on}}} i_{L_{lkg}} dt}{T_s} = (V_{\mathrm{LED1}} + V_{\mathrm{LED2}})\, I_{\mathrm{LED}}. \tag{13}$$

Since $i_{L_{lkg}} = i_{Lm} + n_{i_{D1}}$ during T_{on}, as mentioned in the previous section, and assuming $V_{\mathrm{LED}} = V_{\mathrm{LED1}} = V_{\mathrm{LED2}}$ leads (13) to the following equation:

$$V_{\mathrm{in}} \left[\frac{\int_0^{T_{\mathrm{on}}} i_{Lm} dt}{T_s} + n \frac{\int_0^{T_{\mathrm{on}}} i_{D1} dt}{T_s} \right] = V_{\mathrm{in}} \left[D \langle i_{Lm} \rangle + n I_{\mathrm{LED}} \right] = 2 V_{\mathrm{LED}} I_{\mathrm{LED}} \tag{14}$$

where $\langle i_{Lm} \rangle$ represents $\int_0^{T_s} i_{Lm} dt / T_s$, the average value of i_{Lm}. Then, rearranging (14) leads to the following equation:

$$\langle i_{Lm} \rangle = \frac{I_{\mathrm{LED}}}{D} \left(\frac{2 V_{\mathrm{LED}}}{V_{\mathrm{in}}} - n \right). \tag{15}$$

Since $2V_{\mathrm{LED}}/V_{\mathrm{in}} = n/(1-D)$ according to the voltage conversion ratio

$$\langle i_{Lm} \rangle = \frac{n I_{\mathrm{LED}}}{1-D}. \tag{16}$$

The boundary conduction mode (BCM) occurs when $\langle i_{Lm} \rangle = \Delta i_{Lm}/2$. Since $\Delta i_{Lm} = V_{\mathrm{in}} D T_s / L_m$ according to the previous mode analysis, BCM condition can be derived as follows:

$$L_m = \frac{V_{\mathrm{in}} D (1-D) T_s}{2 n I_{\mathrm{LED}}}. \tag{17}$$

Rearranging (7) and (17) leads to the following equation:

$$L_m = \frac{V_{\mathrm{in}} T_s}{4 I_{\mathrm{LED}} V_{\mathrm{LED}}} \left(1 - \frac{n V_{\mathrm{in}}}{2 V_{\mathrm{LED}}} \right). \tag{18}$$

The selection of L_m and f_s is related to the efficiency optimization of the proposed converter. Optimizing process of the proposed converter is very similar with the conventional flyback converter. For L_m, larger L_m leads to reduced conduction loss because of small RMS current. On the other hand, the core size and loss increase because of high total flux linkage in the transformer. For switching frequency, smaller f_s leads to the reduced number of the hard switching transition. However, too small switching frequency leads to a high peak turn-off current of the main switch, resulting in high switching turn-off energy and large RMS current. In this example, considering the tradeoffs, 3.3 V input and 0.175 A (50% of rated current) condition with 70 kHz switching frequency is selected to BCM condition. Substituting $V_{\mathrm{in}} = 3.3$ V, $T_s = 1/70$ K, $I_{\mathrm{LED}} = 0.75$ A, and $V_{\mathrm{LED}} = 15.386$ V leads to $L_m = 6\,\mu$H. Considering the peak of $i_{Lm} = \langle i_{Lm} \rangle + \Delta i_{Lm}/2$ occurs at the minimum input and the maximum output condition, Kool-mu 77059 has been selected as the transformer core. In order to maximize the efficiency of the transformer, the windings of the transformer have been wound as tight as possible. L_{lkg} value can be obtained by measuring the resonant frequency from the waveforms. As a result, $N_p = 12$, $N_s = 61$, $n = 5.08$, $L_m = 6.25\,\mu$H, and $L_{lkg} = 80$ nH transformer has been designed.

D. Resonant Blocking Capacitor

The resonant frequency of the proposed driver can be selected considering the efficiency. When the proposed converter has a long resonant period, it operates in an above region. In this case, a large turn-off current in the main switch and reverse recovery loss in the rectifier diode deteriorate the efficiency. On the other hand, in a deep below region, RMS current increases in order to deliver the same amount of charge in a short resonant period. Therefore, the capacitance of the blocking capacitor has been seen selected to obtain the resonant point operation at the maximum input voltage (where DT_s is the minimum) and 0.35 A output condition. In order to have the resonant point operation, C_b is selected so that DT_s should be equal to the half resonant period as follows:

$$DT_s = \pi\sqrt{(n^2 L_{lkg})C_b} \tag{19}$$

$$C_b = \frac{D^2}{n^2\pi^2 {f_s}^2 L_{lkg}} = \frac{1}{n^2\pi^2 {f_s}^2 L_{lkg}}\left(1 - \frac{nV_{\text{in\_max}}}{V_{\text{LED1}} + V_{\text{LED2}}}\right)^2. \tag{20}$$

In this example, $C_b = 2.11\,\mu\text{F}$ with $n = 5$, $f_s = 70\,\text{kHz}$, $L_{lkg} = 80\,\text{nH}$, $V_{\text{in\_max}} = 3.63\,\text{V}$, and $2V_{\text{LED}} = V_{\text{LED1}} + V_{\text{LED2}}$. Therefore, 2.2 μF MLCC capacitor has been selected as the blocking capacitor.

E. Output Capacitor

The output capacitors can be selected considering the output ripple current ΔI_{LED}. In the proposed converter, the output ripple voltage ΔV_{LED} is equal to $I_{\text{LED}}T_s/C_o$, same with the conventional flyback converter. Also, since $\Delta I_{\text{LED}} = \Delta V_{\text{LED}}/R_{\text{LED}}$ from the piecewise linear model, the required C_o can be obtained by rearranging these two equations as follows:

$$C_o = \frac{I_{\text{LED}}}{\Delta I_{\text{LED}}}\frac{1}{R_{\text{LED}} f_s}. \tag{21}$$

In this example, $C_o = 42.5\,\mu\text{F}$ with $\Delta I_{\text{LED}} = 0.05 I_{\text{LED}}$, $R_{\text{LED}} = 6.72\,\Omega$, and $f_s = 70\,\text{kHz}$. Therefore, two 22 μF MLCCs are used for each output capacitor.

E. Main Switch

In the flyback type converters, the maximum voltage stress is calculated including the voltage spike in order to have sufficient margin to the voltage rating of the main switch. From the previous analysis, the peak voltage stress on the main switch is equal to $V_{\text{LED2}} + v_{cb}(t_2)$. Substituting (7) and (9) into (11) leads to the maximum voltage stress on the main switch as follows:

$$V_{Q\_\max} = V_{\text{LED1}} + V_{\text{LED2}} - nV_{\text{in}} - \frac{I_{\text{LED}}}{2C_b f_s} \tag{22}$$

$$V_{Q\_\max} = 2V_F - nV_{\text{in}} + \left(2R_{\text{LED}} - \frac{1}{2C_b f_s}\right) I_{\text{LED}}. \tag{23}$$

In this example, $2R_{\text{LED}} - 1/2; C_b f_s$ is positive as 3.25 with $R_{\text{LED}} = 6.72\,\Omega$, $C_b = 2.2\,\mu\text{F}$, and $f_s = 70\,\text{kHz}$. Therefore, it can be noted that the maximum voltage stress on the main switch occurs at the minimum input voltage and the maximum output current condition. With $V_{\text{in}} = 2.97\,\text{V}$ and $I_{\text{LED}} = 0.35\,\text{A}$, the maximum voltage stress on the switch becomes 17.1 V. With sufficient margin, IPB017N08N5 (70 V, 1.7 mΩ) main switch has been selected. Considering that a switch with a lower voltage rating usually has a smaller turn-on resistance, the efficiency of the proposed converter can be improved further with 30 V rated switches.

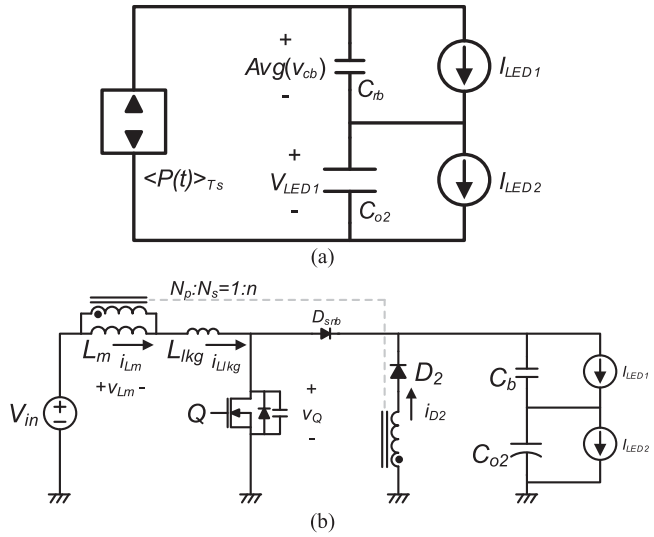

Fig. 9. (a) Equivalent power deliver model and (b) small-signal equivalent flyback converter of the proposed converter.

F. Control to Output Transfer Function

In order to discuss about the current control of the proposed driver, the small-signal modeling of the proposed driver should be provided. The control to output transfer function of the proposed driver can be obtained in a similar way with a conventional flyback converter in CCM, excepting that C_b is series connected with the output capacitors. Therefore, we would like to show an equivalent flyback converter, which has the same control to output function with the proposed converter.

In the proposed converter, the amount of charge delivered to channel 1 while the main switch is turned on is equal to the amount of charge delivered to the blocking capacitor while the main switch is turned off. Therefore, channel 1 can be considered as the load of the blocking capacitor, and Fig. 9 represents the equivalent power deliver model and the small-signal equivalent flyback converter of the proposed driver which has the same control to output transfer function with the proposed converter [10]. $\langle P(t)\rangle_{\text{Ts}}$ represents the average delivered power to the output side. Fig. 10 represents the simulation results of the control to output transfer functions of the proposed driver and the equivalent converter in Fig. 9(b). The blue and red solid lines represents the control to output transfer functions for channels 1 and 2, respectively. The black dotted line represents the control to output transfer function for channel 2 of the equivalent flyback converter. From the simulation results, it can be noted that the equivalent flyback converter provides a quite exact control to output transfer function. Therefore, it can be noted that the

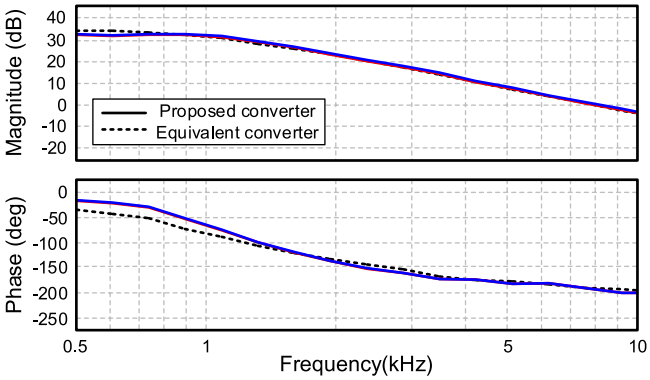

Fig. 10. Simulation results of the control to output transfer function.

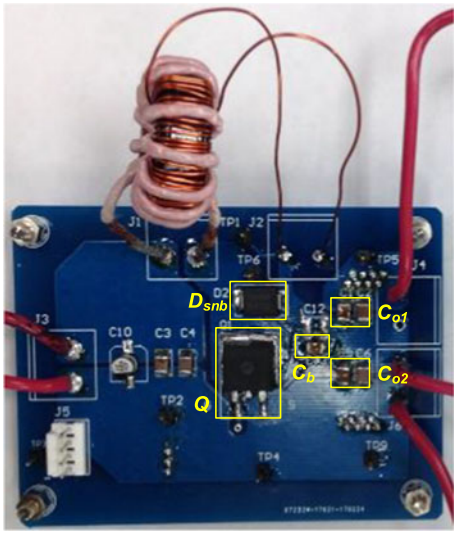

Fig. 11 Prototype of the proposed driver.

small-signal modeling of the flyback converter in Fig. R2(b) lead us to the control to output function of the proposed driver. The small-signal LED current can be obtained by dividing the control to output transfer function by the LED resistance

$$\frac{\hat{i}_{\mathrm{LED}}}{\hat{d}} = \frac{\hat{v}_{\mathrm{LED}}}{\hat{d}} \frac{1}{R_{\mathrm{LED}}}. \tag{24}$$

Therefore, the current controller can be design for the proposed driver with the simple flyback converter modeling.

V. Experimental Results

Fig. 11 and 12 illustrate the prototype of the proposed driver and the key waveforms with the rated output current at different input voltage conditions. In accordance with the design example, the duty ratio of the proposed driver is near 0.5 at $V_{\mathrm{in}} = 3.3\,\mathrm{V}$ and the rated output current condition. The duty ratio slightly higher/lower than 0.5 in the case of $V_{\mathrm{in}} = 2.97\,\mathrm{V}$ and $V_{\mathrm{in}} = 3.63\,\mathrm{V}$ conditions, respectively. Therefore, the average value of v_{Cb} is near zero, and Δv_{Cb} is the same in all cases as analyzed before. Also, v_{Cb} decreases during DT_s so that the voltage stress on the main switch is further suppressed. The proposed converter operates at the resonant point at $V_{\mathrm{in}} = 3.63\,\mathrm{V}$,

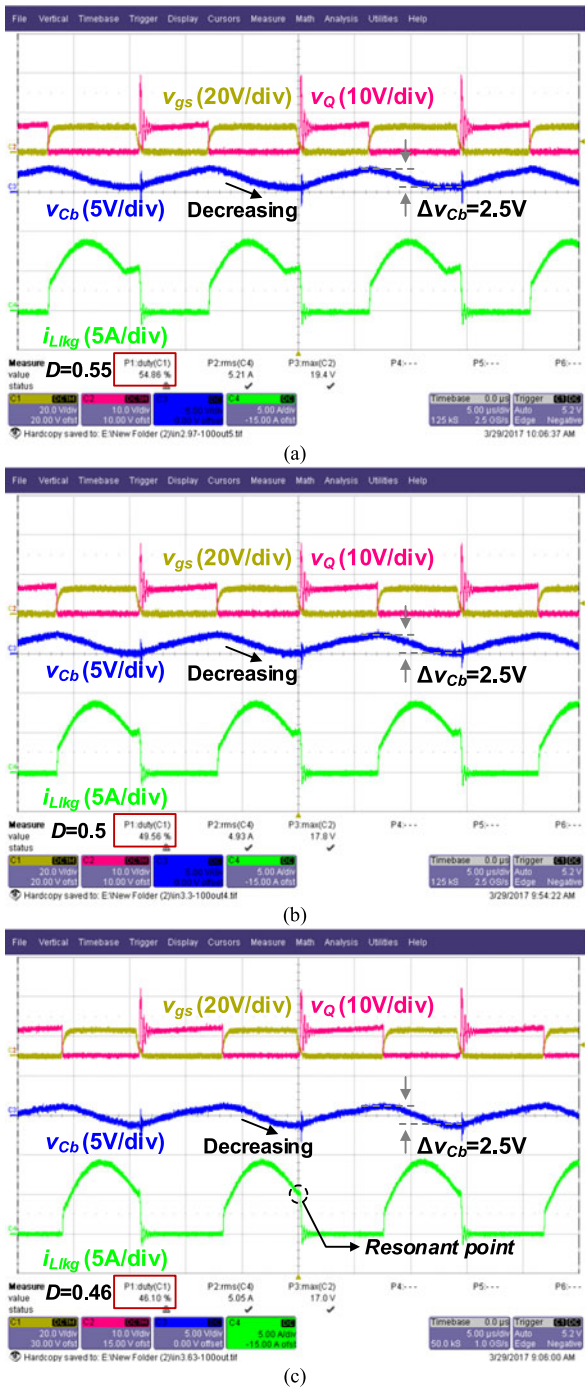

Fig. 12. Key waveforms with the rated output current (0.35 A) at (a) $V_{\mathrm{in}} = 2.97\,\mathrm{V}$, (b) $V_{\mathrm{in}} = 3.3\,\mathrm{V}$, and (c) $V_{\mathrm{in}} = 3.63\,\mathrm{V}$.

as shown in Fig. 10(c). From the waveforms, it can be noted that the proposed converter has small turn-off switching current regardless of the input voltage condition. This is because the proposed converter is a resonant type, whereas the conventional converters [15], [16] have a higher switching turn-off current at a lower input voltage conditions.

Fig. 13 illustrates zoomed in waveforms for $V_{Q\_\max}$ with the rated output current at different input voltage conditions. Figs. 12(a) and 13(a), 12(b) and 13(b), and 12(c) and 13(c)

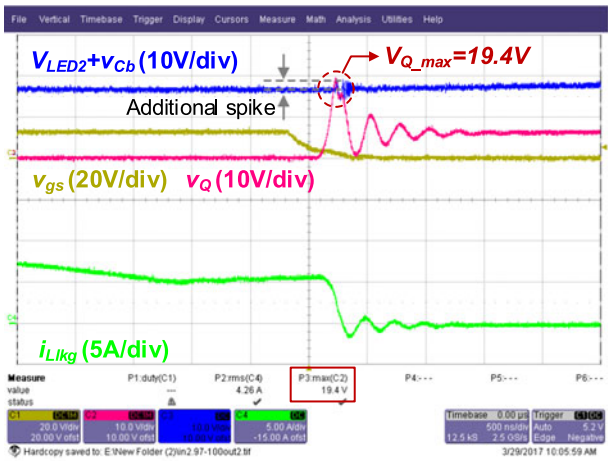

(a)

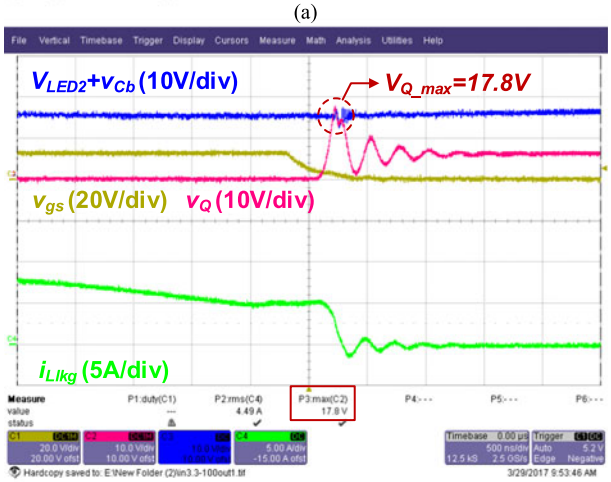

(b)

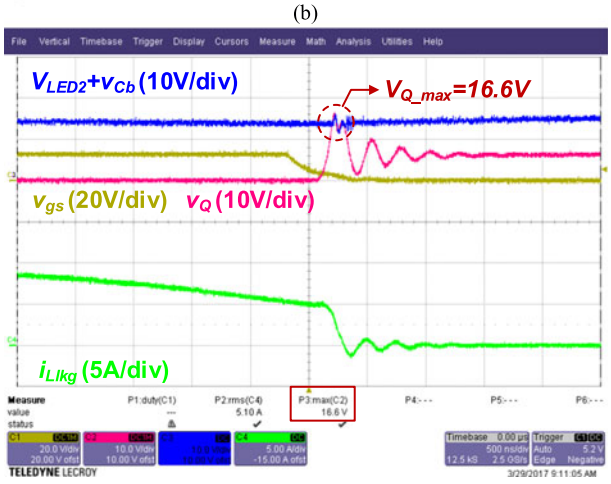

(c)

Fig. 13. Zoomed-in waveforms for V_{Q_max} with 0.35 A output current at (a) $V_{in} = 2.97$ V, (b) $V_{in} = 3.3$ V, and (c) $V_{in} = 3.63$ V.

are the experimental waveforms with the same operating conditions, respectively. As analyzed before, V_{Q_max} becomes higher as the input voltage decreases and the worst condition occurs at $V_{in} = 2.97$ V. The maximum V_{Q_max} was 19.4 V with the experiment, whereas the analysis result was 17.1 V. This is due to the additional voltage spike caused by the turn-on delay time of the snubber diode and the parasitic components such as parasitic inductor and resistor in the clamping loop.

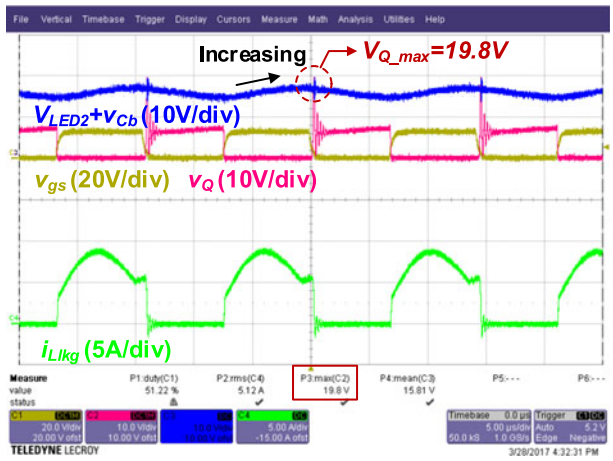

Fig. 14. Increased V_{Q_max} with the opposite connection of N_s at $V_{in} = 3.3$ V and 0.35 A output current.

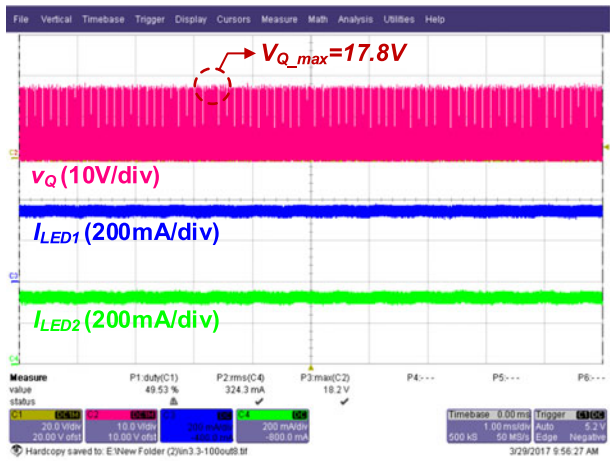

(a)

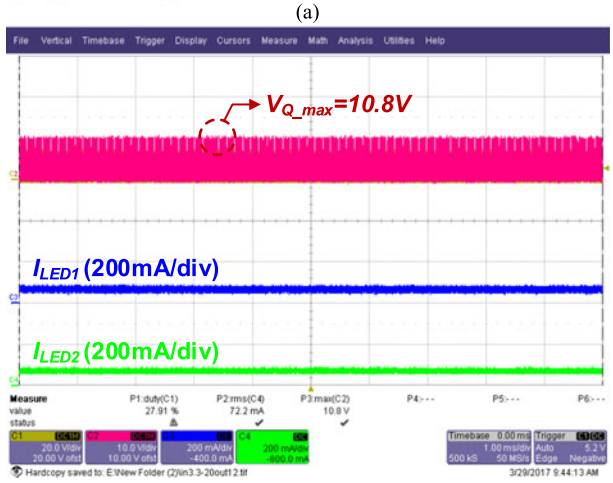

(b)

Fig. 15. Current sharing capability and V_{Q_max} of the proposed converter at $V_{in} = 3.3$ V: (a) 0.35 A and (b) 0.07 A output current conditions.

Fig. 14 illustrates V_{Q_max} with the opposite connection of N_s at $V_{in} = 3.3$ V and the rated output current condition. As shown in the figure, v_{Cb} increases during DT_s and V_{Q_max} has been increased by 2 V compared to Fig. 11(b).

Fig. 15 illustrates the current sharing capability and V_{Q_max} of the proposed converter at $V_{in} = 3.3$ V with 100% and 20% of

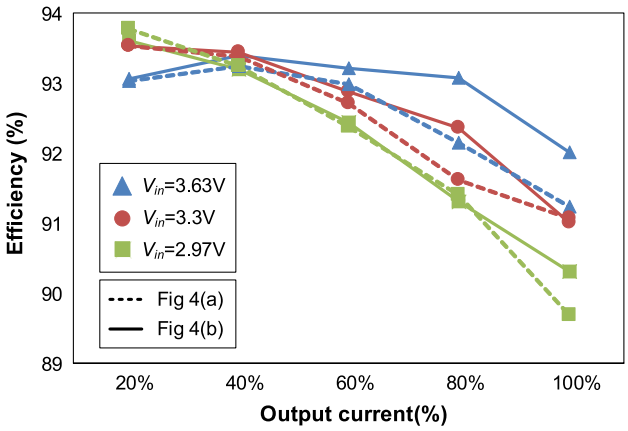

Fig. 16 Measured efficiency of the proposed converters.

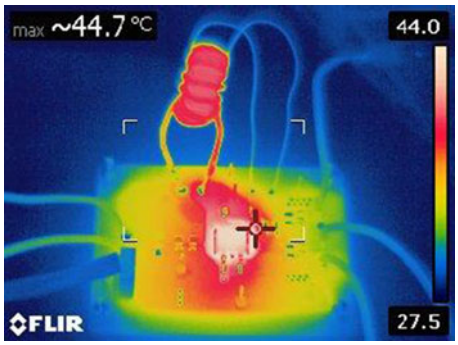

Fig. 17. Temperature of the proposed converter at 2.97 V and 0.35 A condition (1-h aging without heatsink and airflow).

the rated output current. As shown in the figure, current in both channels are shared equally in the entire load conditions. V_{Q_max} decreases as the output current decreases as analyzed before.

Fig. 16 illustrates the efficiency of the proposed converter. The dotted and solid lines represent the efficiency of the proposed converter in Fig. 4(a) and (b), respectively. The difference is the voltage stress on the main switch. As mentioned before, in the proposed converter in Fig. 4(a), the voltage stress on the main switch becomes $V_{\mathrm{LED1}} + V_{\mathrm{LED2}}$. On the other hand, in the proposed converter in Fig. 4(b), the voltage stress on the main switch becomes smaller than Fig. 4(a). Also, the maximum voltage stress on the main switch occurs during the switching turn-off transition. Therefore, the main switch of the proposed convert can have lower switching turn-off loss, resulting in a higher efficiency. As shown in Fig. 14, the proposed converter has a high efficiency in the entire input and output conditions. In almost every conditions, the efficiency of the proposed converter is higher than 90%.

Fig. 17 illustrates the temperature of the proposed converter at 2.97 V and 0.35 A condition after 1 h aging without heatsinks and airflow. The highest temperature 44 °C is observed at the main switch, and it can be noted that the proposed converter is thermally stable.

Table II illustrates the comparison on the number of components. As shown in the table, the proposed converter has the minimized number of components since it does not have the snubber capacitor and uses one main switch. Furthermore, the snubber diode has a small average current since it is turned on only when $i_{L_{lkg}}$ is reset. On the other hand, the snubber diode in [15] has 0.35 A channel current as its average current.

TABLE II
COMPARISON ON THE NUMBER OF MAIN COMPONENTS

Components	Proposed	[3]	[4]
Magnetic component	1	1	1
Blocking cap.	1	1	1
Main switch	1	1	2
Rectifier diodes	2	2	2
Snubber diode (Avg. current)	1 (<0.05 A)	1 (0.35 A)	-
Snubber capacitor	-	1	1
Total	6	7	7

VI. CONCLUSION

In this paper, a new single-switch nonisolated two-channel LED driver for low output power has been proposed and analyzed. The proposed converter uses the blocking capacitor and the output capacitor as the snubber capacitor. By doing so, the proposed converter eliminates the snubber capacitor while maintaining the current sharing capability. Also, the proposed converter has a low-voltage stress on the main switch. Furthermore, the proposed converter can achieve a high efficiency since it has smaller number of components in the main current path and smaller main switch turn-off current due to the resonance. Therefore, the proposed converter can be a strong candidate in the small power LED driver applications.

REFERENCES

[1] H. J. Chiu and S. J. Cheng, "LED backlight driving system for large-scale LCD panels," *IEEE Trans. Ind. Electron.*, vol. 54, no. 5, pp. 2751–2760, Oct. 2007.
[2] Y.-K. Lo, K.-H. Wu, K.-J. Pai, and H.-J. Chiu, "Design and implementation of RGB LED drivers for LCD backlight modules," *IEEE Trans. Ind. Electron.*, vol. 56, no. 12, pp. 4862–4871, Dec. 2009.
[3] X. Wu, Z. Wang, and J. Zhang, "Design considerations for dual-output quasi-resonant flyback LED driver with current-sharing transformer," *IEEE Trans. Power Electron.*, vol. 28, no. 10, pp. 4820–4830, Oct. 2013.
[4] R. Zhang and H. S. Chung, "Use of daisy-chained transformers for current-balancing multiple LED strings," *IEEE Trans. Power Electron.*, vol. 29, no. 3, pp. 1418–1433, Mar. 2014.
[5] W. Yu, J.-S. Lai, H. Ma, and C. Zheng, "High-efficiency dc–dc converter with twin bus for dimmable LED lighting," *IEEE Trans. Power Electron.*, vol. 26, no. 8, pp. 2095–2100, Aug. 2011.
[6] Y. Hu and M. M. Jovanovic, "A new current-balancing method for paralleled LED strings," in *Proc. 26th Annu. IEEE APEC*, Mar. 2011, pp. 705–712.
[7] S. M. Baddela and D. S. Zinger, "Parallel connected LEDs operated at high frequency to improve current sharing," in *Proc. Conf. Rec. 39th IEEE IAS Annu. Meeting*, Oct. 2004, vol. 3, pp. 1677–1681.
[8] J. Zhang, J. Wang, and X. Wu, "A capacitor-isolated LED driver with inherent current balance capability," *IEEE Trans. Ind. Electron.*, vol. 59, no. 4, pp. 1708–1716, Apr. 2012.
[9] X. Wu, J. Zhang, and Z. Qian, "A simple two-channel LED driver with automatic precise current sharing," *IEEE Trans. Ind. Electron.*, vol. 58, no. 10, pp. 4783–4788, Oct. 2011.
[10] J.-W. Kim, J.-P. Moon, and G.-W. Moon, "Analysis and design of a single-switch forward-flyback two-channel LED driver with resonant-blocking capacitor," *IEEE Trans. Power Electron.*, vol. 31, no. 3, pp. 2314–2323, Mar. 2016.

[11] X. Wu, C. Hu, J. Zhang, and C. Zhao, "Series-parallel autoregulated charge-balancing rectifier for multioutput light-emitting diode driver," *IEEE Trans. Ind. Electron.*, vol. 58, no. 10, pp. 4783–4788, Oct. 2011.
[12] J. Zhang, L. Xu, X.Wu, and Z. Qian, "A precise passive current balancing method for multioutput LED drivers," *IEEE Trans. Power Electron.*, vol. 26, no. 8, pp. 2149–2159, Aug. 2011.
[13] C. Zhao, X. Xie, and S. Liu, "Multi-output LED drivers with precise passive current balancing," *IEEE Trans. Power Electron.*, vol. 28, no. 3, pp. 1438–1448, Mar. 2013.
[14] J.-W. Kim, J.-P. Moon, and G.-W. Moon, "Duty-ratio-control-aided LLC converter for current balancing of two-channel LED driver," *IEEE Trans. Ind. Electron.*, vol. 64, no. 2, pp. 1178–1184, Feb. 2017.
[15] K. I. Hwu and W. Z. Jiang, "Single-switch coupled-inductor-based two-channel LED driver with a passive regenerative snubber," *IEEE Trans. Power Electron.*, vol. 32, no. 6, pp. 4482–4490, Jun. 2017.
[16] K. I. Hwu and W. Z. Jiang, "Nonisolated two-channel LED driver with automatic current balance and zero-voltage switching," *IEEE Trans. Power Electron.*, vol. 31, no. 12, pp. 8359–8370, Dec. 2016.
[17] K.-C. Tseng, J.-Ze Chen, J.-T. Lin, C.-C. Huan, and T.-H. Yen, "High step-up interleaved forward-flyback boost converter with three-winding coupled inductors," *IEEE Trans. Power Electron.*, vol. 30, no. 9, pp. 4696–4703, Sep. 2015.
[18] J.-H. Lee, J.-H. Park, and J.-H. Jeon, "Series-connected forward–flyback converter for high step-up power conversion," *IEEE Trans. Power Electron.*, vol. 26, no. 12, pp. 3629–3641, Dec. 2011.
[19] A. Abramonitz and K. M. Smedley, "Analysis and design of a tapped-inductor buck–boost PFC rectifier with low bus voltage," *IEEE Trans. Power Electron.*, vol. 26, no. 9, pp. 2637–2649, Sep. 2011.
[20] S.-W. Lee and H.-Lark Do, "Single-stage bridgeless AC–DC PFC converter using a lossless passive snubber and valley switching," *IEEE Trans. Ind. Electron.*, vol. 63, no. 10, pp. 6055–6063, Oct. 2016.
[21] G. Tibola, E. Lemmen, J. L. Duarte, and Ivo Barbi, "Passive regenerative and dissipative snubber cells for isolated SEPIC converters: Analysis, Design, and Comparison," *IEEE Ind. Power Electron.*, vol. 32, no. 12, pp. 9210–9222, Dec. 2017, to be published.
[22] Texas Instruments, "Design review: Isolated 50 Watt flyback converter using the UCC3809 primary side controller and the UC3965 precision reference and error amplifier," Appl. note U-165, 1999.
[23] D. Shmilovitz, A. Abramovitz, and I. Reichman, "A family of bridgeless quasi-resonant LED drivers," *IEEE Trans. Power Electron.*, vol. 31, no. 3, pp. 1833–1836, Mar. 2016.
[24] D. Shmilovitz, A. Abramovitz, and I. Reichman, "Quasi-Resonant LED Driver With Capacitive Isolation and High PF," *IEEE J. Emerg. Sel. Topics Power Electron*., vol. 3, no. 3, pp. 1833–1836, Sep. 2015.

Jong-Woo Kim (S'13–M'17) received the B.S. and M.S. degrees in electrical engineering from the Korea Advanced Institute of Science and Technology (KAIST), Daejeon, South Korea, in 2010, 2012, and 2016, respectively.

He is currently working as a Postdoctoral Associate at the Future Energy Electronics Center, Virginia Tech, Blacksburg, VA, USA. His current research interests include high-efficiency converter topologies, analog/digital control, server power system, LED power system, and induction cookware system.

Jung-Muk Choe (S'12–M'14) received the B.S., M.S., and Ph.D. degrees in electrical engineering from Konkuk University, Seoul, Korea, in 2008, 2010, and 2014, respectively.

From 2010 to 2011, he was a Researcher at LSIS, Korea. He is currently a Postdoctoral Researcher at the Virginia Polytechnic Institute and State University (Virginia Tech), Blacksburg, VA, USA. His current research interests include the design of high-power converters.

Dr. Choe received a Contribution Award from the *Journal of Power Electronics*, a Contribution Award and an Academic Award from Konkuk University.

Jih-Sheng (Jason) Lai (S'85–M'89–SM'93–F'07) received the M.S. and Ph.D. degrees in electrical engineering from the University of Tennessee, Knoxville, TN, USA, in 1985 and 1989, respectively.

In 1989, he joined the Electric Power Research Institute (EPRI) Power Electronics Applications Center (PEAC), where he managed EPRI-sponsored power electronics research projects. In 1993, he then join the Oak Ridge National Laboratory as the Power Electronics Lead Scientist, where he initiated a high-power electronics program and developed several novel high-power converters, including multilevel converters and soft-switching inverters. In 1996, he joined the Virginia Polytechnic Institute and State University, where he is currently the James S. Tucker Professor in Electrical and Computer Engineering Department and Director of the Future Energy Electronics Center. He also holds Honorary International Chair Professorship at the National Taipei University of Technology, Taiwan, and serves as a Visiting Professor at Nanyang Technological University, Singapore. His current research interests include high-efficiency power electronics conversions for high-power and energy applications. He has authored and coauthored more than 400 refereed technical papers and 2 books and received 25 U.S. patents.

Dr. Lai received the Technical Achievement Award in Lockheed Martin Award Night, 2 Journal Paper Awards, 12 Best Paper Awards from IEEE-sponsored conferences, and Virginia Tech Dean's Award on Research Excellence. He was the recipient of 2016 IEEE IAS Gerald Kliman Innovator Award. He led the student teams to win the Top Three Finalist in Google Little Box Challenge in 2016, the Grand Prize Award from International Future Energy Challenge (IFEC) in 2011, and the Grand Prize Award from Texas Instruments Engibous Analog Design Competition in 2009. He is the Founding Chair of the 2001 IEEE Future Energy Challenge (IFEC) and the 2016 IEEE Asian Conference on Energy, Power, and Transportation Electrification (ACEPT) and the General Chair of the IEEE Workshop on Computers in Power Electronics (COMPEL 2000) and the IEEE Applied Power Electronics Conference and Exposition (APEC 2005).